Journal of Molecular Structure 1225 (2021) 129072

Contents lists available at ScienceDirect

Journal of Molecular Structure

journal homepage: www.elsevier.com/locate/molstr

Synthesis, structural, molecular docking and spectroscopic studies of (*E*)-*N*'-(4-methoxybenzylidene)-5-methyl-*1H*-pyrazole-3-carbohydrazide

Khalid Karrouchi[a,*], Silvia A. Brandán[b,*], Yusuf Sert[c], Miloud El Karbane[a], Smaail Radi[d], Marilena Ferbinteanu[e], Yann Garcia[f], M'hammed Ansar[g]

[a] *Laboratory of Analytical Chemistry and Bromatology, Faculty of Medicine and Pharmacy, Mohammed V University, Rabat, Morocco*
[b] *Cátedra de Química General, Instituto de Química Inorgánica, Facultad de Bioquímica, Química y Farmacia, Universidad Nacional de Tucumán, Ayacucho 471, 4000, Tucumán, Argentina*
[c] *Sorgun Vocational School, Science and Art Faculty-Department of Physics, Yozgat Bozok University, Yozgat, Turkey*
[d] *Laboratory of Applied Chemistry and Environment (LCAE), Department of Chemistry, Faculty of Sciences, Mohammed I University, Oujda 60000, Morocco*
[e] *Inorganic Chemistry Department, Faculty of Chemistry, University of Bucharest, Dumbrava Rosie 23, Bucharest 020462, Romania*
[f] *Institute of Condensed Matter and Nanosciences, Molecular Chemistry, Materials and Catalysis (IMCN/MOST), Université catholique de Louvain, Place L. Pasteur 1, 1348 Louvain-la-Neuve, Belgium*
[g] *Laboratory of Medicinal Chemistry, Faculty of Medicine and Pharmacy, Mohammed V University, Rabat, Morocco*

ARTICLE INFO

Article history:
Received 1 June 2020
Revised 1 August 2020
Accepted 11 August 2020
Available online 13 August 2020

Keywords:
Pyrazole
Crystal structure
NBO
AIM
Hirshfeld surface
Molecular docking

ABSTRACT

(*E*)-*N*'-4-methoxybenzylidene-5-methyl-*1H*-pyrazole-3-carbohydrazide (**E-MBPC**) has been synthesized and characterized by FT-IR, ^{1}H & ^{13}C NMR and ESI-MS spectroscopic methods. The (*E*)-configuration of hydrazonoic group was confirmed by single-crystal X-ray diffraction. Theoretical structures of **E-MBPC** in both gas phase and aqueous solution have been optimized by using hybrid B3LYP/6-311++G** calculations. Calculations in solution have shown that dipole moment increases from 7.97 D in the gas phase to 13.68 D in solution with solvation energy of −131.34 kJ/mol. Atomic charges have evidenced that the protonation of **E-MBPC** in solution could occur only in the N28 atom because those charges on this atom show negative values. Mapped MEP surfaces show that the nucleophilic sites is located on the O21 and N28 atoms including the N16 atom while the electrophilic sites are observed on the N24-H27 and N18-H19 bonds. NBO calculations support the high stability of **E-MBPC** in solution while frontier orbitals studies suggest low reactivity of **E-MBPC** in both media, as compared with the (*E*)-*N*'-(4-(dimethylamino)benzylidene)-5-methyl-*1H*-pyrazole-3-carbohydrazide derivative. The vibrational assignments of 93 vibration modes expected for **E-MBPC** were reported together with the corresponding force fields and force constants in both media. The predicted Raman and Ultraviolet-visible spectra were also reported for **E-MBPC** at the same level of theory. Good correlations were obtained between the predicted ^{1}H- and ^{13}C NMR spectra and the corresponding experimental ones. In addition, molecular docking studies between the title ligand and 4AMJ protein were performed. Docking results revealed that the title compound can be designed as a potential anti-diabetic agent.

1. Introduction

Studies of pyrazole derivatives have become of much interest because among a wide variety of heterocycles these species are investigated for the development of new active molecules [1]. A systematic investigation of this class of compounds revealed that pyrazole can be traced in a number of well-established drugs belonging to different categories with diverse pharmacological activities [2–6] and pesticides [7,8] (Fig. 1). Pyrazole derivatives have a wide range of biological activities, antifungal and pesticidal agents, among other [9–21] while compounds with hydrazone moiety represent an important class of organic compounds, especially in medicinal and pharmaceutical chemistry [22,23]. In view of the pharmacological importance of pyrazole derivatives, the investigation of their molecular geometric structure, electronic and thermodynamic properties are fundamental to know the influence of different groups on structures in order to discover the relationship of these groups with their biological properties. In this con-

* Corresponding authors.
E-mail addresses: khalid.karrouchi@um5s.net.ma (K. Karrouchi), brandansa@yahoo.com.ar (S.A. Brandán).

https://doi.org/10.1016/j.molstruc.2020.129072
0022-2860/

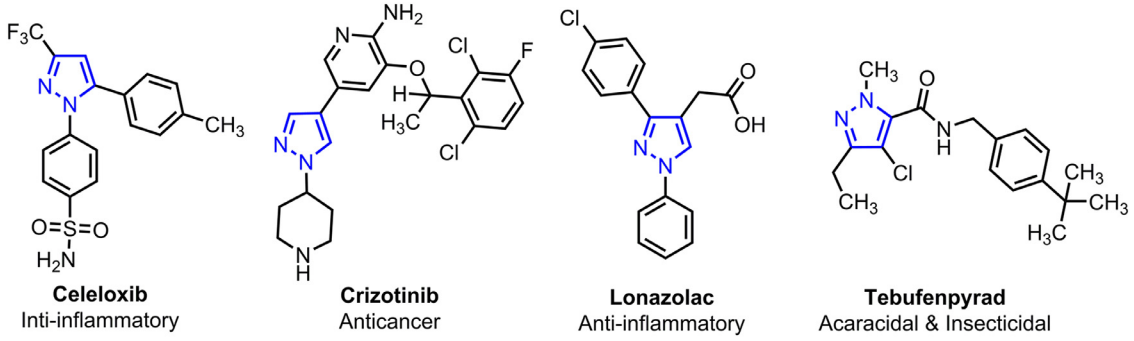

Fig. 1. Selected examples of pharmaceutically relevant pyrazoles.

text, DFT calculations have become a very important and frequently used tool to develop a close relationship between theoretical and experimental data by giving clues related to molecular geometry, spectroscopic (FT-IR, Raman, UV–vis and ^{1}H & ^{13}C NMR chemical shifts) electronic and thermodynamic properties. Consequently, these techniques have become very reliable in predicting the properties of molecules with great precision [24–28].

In this study, we report the synthesis of a new molecule containing both pyrazole and hydrazone groups: (*E*)-*N*'-4-methoxybenzylidene-5-methyl-*1H*-pyrazole-3-carbohydrazide (**3**) . This compound was fully characterized by IR, ^{1}H NMR, ^{13}C NMR, EIS-MS spectrometry and single-crystal X-ray diffraction. Furthermore, DFT calculations were carried in order to study the molecular geometric structure, vibrational frequencies, ^{1}H & ^{13}C NMR chemical shifts, HOMO-LUMO energies, NBO, AIM and molecular electrostatic potential (MEP) using DFT/B3LYP method with 6-311++G(d,p) basis. In addition, Hirshfeld surface analyses were performed to understanding molecular packing and possible bonding. One of the most important targets of computational chemistry is to determine the tendency of enzymes and proteins to bind small molecules. Molecular docking is used to locate small molecules in the active site of the target protein in other words the lowest energy conformation of the ligand in the binding package of the protein is investigated and scored, therefore lastly the molecular docking analyses were investigated between (*E*)-*N*'-4-methoxybenzylidene-5-methyl-1H-pyrazole-3-carbohydrazide (E-MBPC) and PDB: 4AMJ protein.

2. Experimental section

2.1. General methods

All chemical reactions were purchased Sigma-Aldrich. Reactions were checked with TLC using aluminum sheets with silica gel 60 F254 from Merck. Melting points were measured using a Buchi B-545 digital capillary melting point apparatus and used without correction. The FT-IR spectrum of solid was recorded in reflectance (ATR) mode with a Perkin-Elmer VERTEX 70 FT-IR spectrometer covering field 400–4.000 cm^{-1}. ^{1}H and ^{13}C NMR spectra were recorded in solution in DMSO-d_6, on Bruker spectrometer (300 MHz). The chemical shifts are expressed in parts per million (ppm) by using tetramethylsilane (TMS) as internal reference. Mass spectra were collected using API 3200 LC/MS/MS system, equipped with an ESI source.

2.2. Synthesis

General procedure for the synthesis of (E)-N'-(4-metoxybenzylidene)-5-methyl-1H-pyrazole-3-carbohydrazide (E-MBPC): Target compound (**E-MBPC)** described here was facilely synthesized according to the literature procedures [29–32] (Scheme 1). To a solution of 5-methyl-*1H*-pyrazole-3-carbohydrazide (**1**) (140 mg, 1 mmol) and 4-methoxybenzaldehyde (**2**) (136 mg, 1 mmol) in ethanol (10 mL) was added two drops of acetic acid. The mixture was maintained under reflux for 2 h. Then, the reaction mixture was poured in cold water, and the precipitate formed was filtered out washed with ethanol and recrystallized from ethanol.

Yield 201 mg, 78%, M.p. 260–262 °C; IR (ATR, ν(cm^{-1})) : 3214 (NH), 1651 (C=O), 1605 (N=CH); ^{1}H-NMR (300 MHz, DMSO-d_6, δ(ppm)): 2.26 (s,3H, CH_3), 3.77 (s, 3H, OCH_3), 6.47 (s, 1H, H-pyrazole), 6.98 (d, J = 8.7 Hz, 2H, H-Ar), 7.60 (d, J = 8.7 Hz, 2H, H-Ar), 8.39 (s, 1H, -NH), 11.44 (s, 1H, N=CH) 13.05 (s, 1H, NH-pyrazole); ^{13}C NMR: (300 MHz, DMSO-d_6, δ (ppm)): 10.80 (CH_3), 55.74 (OCH_3), 105.22 (CH, C4-pyrazole), 114.76 (CH, C2-Ar), 127.55 (CH, C3-Ar), 129.02 (C, C1-Ar), 140.45 (C, C3-pyrazole), 146.45 (CH, N=CH), 147.53 (C, C5-pyrazole), 158.72 (C, C=O) 161.13 (C, C–OCH_3). MS: *m/z* = 259.5 [M + H]$^{+}$, 281.3 [M+Na]$^{+}$.

2.3. Single crystal X-ray diffraction

X-ray single crystal data were collected by using MoKα (λ = 0.71075 Å) radiation on a Rigaku R-Axis Rapid II diffractometer equipped with an large-area curved imaging plate detector (460.0 × 256.0 mm), 3-circle goniometer and high-frequency 5 kW sealed tube. All calculations were performed using the CrystalStructure [33] crystallographic software package except for refinement, which was performed using the software package Olex1.2 [34]. The structure was solved by direct methods and refined in a routine manner (SHELXL) [35]. Non-hydrogen atoms were re-

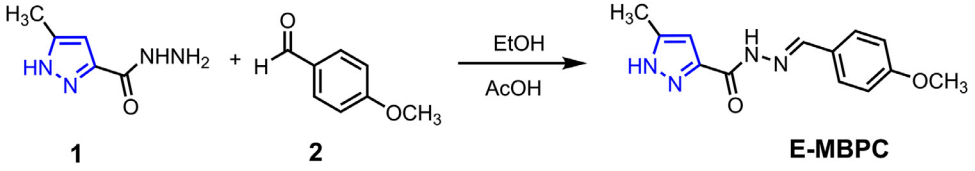

Scheme 1. The synthetic route of compound E-MBPC.

Table 1
Refinement parameters and crystal data for **E-MBPC.**

CCDC Deposition Number	2003254
Crystal data	
Molecular Formula	$C_{13}H_{14}N_4O_2$
Molecular Weight	258.21
Crystal System, Space Group	Monoclinic, $P2_1/c$
Temperature (K)	293
a, *b*, *c* (Å)	6.3744 (2), 20.0589 (7), 10.2754 (7)
β (°)	106.261 (8)
V (Å^3)	1261.29 (12)
Z	4
Dcalc (g•cm^{-3})	1.279
Radiation type	Mo $K\alpha$
μ (mm^{-1})	0.10
Crystal Dimension (mm)	0.60 × 0.15 × 0.10
Data collection	
Diffractometer	Rigaku R-AXIS RAPID II
No. of measured, independent and observed [$F^2 > 2.0\sigma(F^2)$] reflections	10133, 2897, 1790
R_{int}	0.035
(Sin $\theta/\lambda)_{max}$ (Å^{-1})	0.649
Refinement	
$R[F^2 > 2\sigma(F^2)]$, $wR(F^2)$, S	0.045, 0.081, 1.11
No. of reflections	2897
No. of parameters	172
$\Delta\rho_{max}$, $\Delta\rho_{min}$ (e Å^{-3})	0.20, −0.23

fined anisotropically. Hydrogen atoms were refined using the riding model. Molecular graphics were generated by using MERCURY 3.9 [36] and POV-Ray software [37]. The details of the X-ray crystal data and the structure solution as well as the refinement are given in Table 1. A summary of selected bond lengths [Å] and angles [°] are given in Table S1 (ESI). CCDC 2003254 contain the supplementary crystallographic data for the compound, and can be obtained free of charge from the Cambridge Crystallographic Data Centre via www.ccdc.cam.ac.uk/data_request/cif.

2.4. Computational details

The experimental CIF file structure determined by X-ray crystal data for (*E*)-*N*'-(4-methoxybenzylidene)-5-methyl-*1H*-pyrazole-3-carbohydrazide (**E-MBPC**) was taken as initial theoretical one. Then, that structure was optimized in gas phase and in aqueous solution with the hybrid B3LYP/6-311++G** method [38,39] and the Revision A.02 of Gaussian09 program [40]. The self-consistent reaction field (SCRF) methodology with the IEFPCM and universal solvation models were both employed in solution because these schemes consider the solvent effects [41–43] while the volumes and its variations were computed with the Moldraw program [44]. Natural population analysis (NPA) and atomic Merz-Kollman (MK) charges [45], molecular electrostatic potential (MEP) and stabilization energy were predicted in both media with the same level of theory and the version 3.1 of NBO program [46] while the topological properties were calculated with the version 2000 of AIM program [47,48]. The version 5.0 of *GaussView* program was employed to generate the mapped MEP surface of **E-MBPC** [49]. On the other hand, the SQMFF methodology and the version 7.0 of Molvib program were used to calculate the harmonic force fields in both media together with the normal internal coordinates and transferable scaling factors [50–52]. Here, the vibrational assignments were performed considering potential energy distribution (PED) contributions ≥ 10% while the predicted Raman spectrum in activities was transformed to intensities by using known equations [53]. The GIAO method was used to predict the ^{1}H- and ^{13}C-NMR spectra of **E-MBPC** in aqueous solution by using the hybrid B3LYP/6-311++G** method [54] while the electronic spectrum in the same medium was predicted by using NStates=100 and the B3LYP/6-311++G** method with the Time-dependent DFT calculations (TD-DFT) incorporate in the Gaussian09 program [40]. In addition, the frontier orbitals were calculated to predict reactivities of **E-MBPC** in both media by using the B3LYP/6-311++G** level of theory while the behaviours in both media were evaluated with some descriptors of reactivity such as, chemical potential (μ), electronegativity (χ), global hardness (η), global softness (S), global electrophilicity index (ω) and nucleophilicity indexes (E) calculated at the same level of theory [24,26–28,55]. The Hirshfeld surface analysis was performed with Crystal Explorer 3.1 program [56]. In final section, the molecular docking mechanism between the ligand and 4AMJ protein were studied by using AutoDock Vina free software program [57]. The PDBQT formats of ligand and 4AMJ protein were adjusted with Discover Studio Visualizer 4.0 (DSV 4.0) software [58].

Table 2
Calculated total energies (*E*), dipole moments (μ) and volumes (V) for (*E*)-*N*'-4-methoxybenzylidene)-5-methyl-1H-pyrazole-3-carbohydrazide (E-MBPC) in gas and aqueous solution phases by using the B3LYP/6-311++G** Method.

E-MBPC					
B3LYP/6-311++G** Method					
Medium	E (Hartrees)	E_{ZPVE} (Hartrees)	μ (D)	V (Å^3)	ΔV (Å^3)
GAS	-873.4558	-873.1968	7.97	272.0	-1.0
PCM	-873.4960	-873.2361	13.68	271.0	

3. Results and discussion

3.1. X-ray crystal structure description

The compound **E-MBPC** was analyzed by single crystal X-ray diffraction (Fig. 2). The summary of crystallographic information is listed in Table 1. The compound (**E-MBPC)** crystalized in the monoclinic space group $P2_1/c$. The molecule is planar and bond lengths are comparable comparing with the (E)-*N*'-(4-(dimethylamino)benzylidene)-5-methyl-1H-pyrazole-3-carbohydrazide structure published before [55]. The unit cell contains four molecules. The crystal packing (Fig. 3) shows that two by two molecules are arranged in parallel plans within a distance of ~9.407 Å and respective 10.408 Å and there are no supramolecular interactions between them.

3.2. Optimizations and properties in both media

Results of optimizations of (*E*)-*N*'-(4-methoxybenzylidene)-5-methyl-*1H*-pyrazole-3-carbohydrazide (**E-MBPC**) in gas phase and aqueous solution by using the B3LYP/6-311++G** method can be seen in Table 2 while in Fig. 4 is given the optimized structure together with the atoms labelling. The identifications of both rings can also be seen in Fig. 2 where R1 is identified as the phenyl ring while R2 is the pyrazole ring. The relative energy value was obtained from the difference between the value optimized in solution and the corresponding in gas phase (−873.2361+ 873.1968 = −0.0393 Hartrees = 103.08 kJ/mol). Analyzing Table 2 we observed that the calculated total energies (E) in both media show most negatives values, as compared with the corrected values by ZPVE energies (E_{ZPVE}) while the dipole moment (μ) increases from 7.97 D in gas phase to 13.68 D in solution. Hence, probably the cationic species of **E-MBPC** is presents in solution due to notable increase in the dipole moment value while a slight contraction of −1.0 Å^3 in the volume is observed in solution. When the magnitudes and orientations of dipole moment vectors of **E-MBPC** in both media are, the directions and

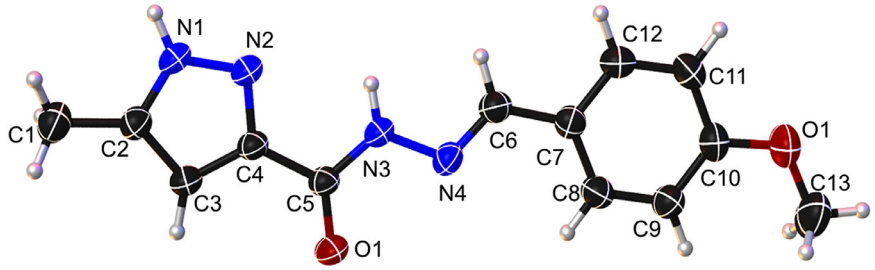

Fig. 2. X-ray molecular structure of the **E-MBPC** compound with atoms numbering scheme. Thermal ellipsoids representation with 50% probability. Olex and POV-Ray representation.

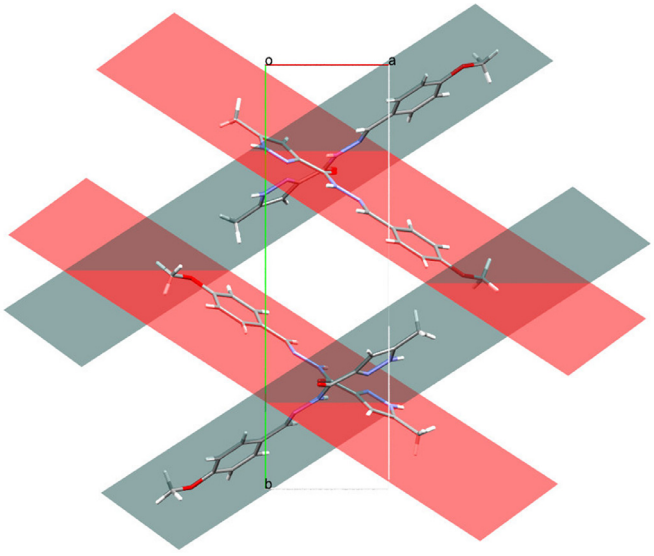

Fig. 3. Crystal packing along c axis-detail of the planar arrangement.

orientations practically remain constants in both media and, only, change in the magnitudes of μ is observed in solution (Fig. S1). The volume contraction observed in solution could be attributed to the hydration of donors (O and N atoms) and acceptors groups (N–H) of H bonds present in the structure of **E-MBPC**. These new H bonds formed in the weak base **E-MBPC** could justify the increase of μ and the volume contraction in solution. The prediction

Table 3
Corrected and uncorrected solvation energies by the total non-electrostatic terms and by zero point vibrational energy (ZPVE) (*E*)-*N*'-4-methoxybenzylidene)-5-methyl-1H-pyrazole-3-carbohydrazide (E-MBPC) in aqueous solution by using the B3LYP/6-311++G** Method.

B3LYP/6-311++G** method[a]			
Solvation energy (kJ/mol)			
Condition	$\Delta G_{un}{}^{\#}$	ΔG_{ne}	ΔG_c
E-MBPC[a]	-103.08	28.26	-131.34
E-MABPC[b]	-105.97	23.53	-129.50

$\Delta G_{un}{}^{\#}$= uncorrected solvation energy; ΔG_{ne}= total non electrostatic terms; ΔG_c= corrected solvation energies.
[a] This work.
[b] From Ref [55] for (E-MABPC) (*E*)-*N*'-(4-(dimethylamino)benzylidene)-5-methyl-*1H*-pyrazole-3-carbohydrazide.

of solvation energy of **E-MBPC** in aqueous solution is important taking into account the presence of donors and acceptors groups in its structure. Hence, corrected and uncorrected solvation energies by total non-electrostatic terms and by zero point vibrational energy (ZPVE) of **E-MBPC** by using the B3LYP/6-311++G** method are presented in Table 3 compared with the value obtained for (*E*)-*N*'-(4-(dimethylamino)benzylidene)-5-methyl-*1H*-pyrazole-3-carbohydrazide (E-MABPC) in the same medium and at the same level of theory [55]. Note that the relative energy value 103.08 kJ/mol corresponds to uncorrected solvation energy value ($\Delta G_{un}{}^{\#}$) from Table 3. A comparison between both structures can be observed in Fig. S2. The results show that the solvation energy value of **E-MBPC** is slightly higher (most negative) than the cor-

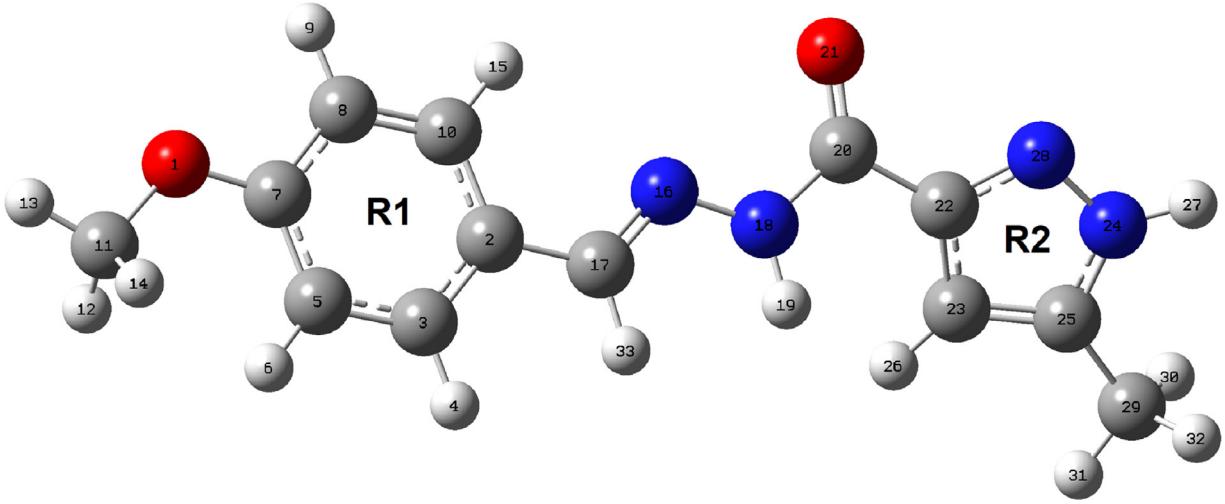

Fig. 4. Theoretical molecular structure of free base of (E)-N'-(4-methoxy)benzylidene)-5-methyl-1H-pyrazole-3-carbohydrazide (**E-MBPC**), atoms labelling and identification of their rings.

responding one to **E-MABPC** probably because in the R1 ring of **E-MBPC,** there is a O–CH_3 group different from E-MABPC where the $N(CH_3)_2$ group is presents in the R1 ring instead of a methoxy group. Besides, the N atom linked to two methyl groups in the latter compound has sp^2 hybridization and both are planar, as shown in Fig. S2. Possibly, these two CH_3 groups in MABPC limit the hydration of water molecules in the N donor as compared to O donor of methoxy group.

Three atomic charges, molecular electrostatic potentials (MEP) and bond orders, expressed as Wiberg indexes are analyzed in the optimized structures of **E-MBPC** in the gas phase and in aqueous solution by using B3LYP/6-311++G** level of theory. Thus, atomic Mulliken, Merz-Kollman and NPA charges, molecular electrostatic potentials (MEP) and bond orders, expressed as Wiberg indexes are summarized in Table S1. Here, these properties are presented and analyzed only for the O and N atoms belonging to donors and acceptors groups of **E-MBPC** in gas phase and in aqueous solution. The behaviours of three studied atomic charges in the different media are shown in Fig. S3. Regarding this latter figure we observed that atomic MK charges on the six considered atoms present slightly different values and behaviours than those predicted for Mulliken and NPA charges. Thus, the Mulliken charges on the N16 atoms belonging to hydrazonoic group of **E-MBPC** in both media have positive and higher values than the other ones while the O21 atoms of C=O bonds present the most negative values as compared with the O1 atoms belonging to methoxy groups. On the other hand, the Mulliken charges predict higher values on the six atoms as compared with the corresponding to NPA ones while the MK charges predict negative values on the six considered atoms and where the O21 and N28 atoms present the higher and most negative values. The three types of charges show that the protonation in aqueous solution could occur only in the N28 atom because the three charges show for these atom negative values while on the N16 atom the Mulliken charges predicted positive values in both media. On the contrary, the three charges predicted that both oxygen atoms can be protonated in solution.

If now the molecular electrostatic potentials (MEP) are evaluated from Table S1, practically the same values are observed in both media and, only the expected tendency is observed, that is, MEP O atoms > MEP N atoms. Particularly, MEP on O21 is > than O1 while MEP N28 present higher values in the two media than the other ones. Hence, these results are in agreement with those observed from the charge's MK and NPA studies. The study of mapped MEP surface is also very important in order to analyze the main reaction sites where the reaction with potential nucleophiles and electrophiles take place. Here, this study was performed for **E-MBPC** in gas phase with the B3LYP/6-31G* method because with the method of higher size failed. In Fig. S4 is presented the calculated electrostatic potential surfaces on the molecular surface of **E-MBPC** in the gas phase with the *GaussView* program [49]. Analyzing the different colorations on the mapped MEP surface, we observed that the intense red colour is located on the two O21 and N28 atoms which have higher MK values including the N16 atom. Hence, the nucleophilic region is wide while other less wide site with weak red colour is observed on the O1 atom. The strong blue colour is observed on the N24-H27 bond and other weak region of the same colour is observed on the other N18-H19 bond, revealing, this way, two clear electrophilic sites.

Other interesting properties analyzed for E-MBPC in both media are the bond orders (BO). In this case they are expressed as Wiberg index and the values are presented in Table S1. The results in both media show few changes in the values where the higher ones are observed for the O1 and N24 atoms. Probably, the higher value observed for the N24 atom is related to the higher lability of H27 atom which is linked to N24 atom. This result is in agreement with the strong blue coloration observed on the N24-H27 bond when the mapped MEP surface is graphed in Fig. S4. The BO values in solution undergo a slight decrease, with exception of the N18 and N24 atoms. Possibly, the hydration with water molecules justifies these variations of the BO in solution.

Table 4
Comparisons of calculated geometrical parameters of (*E*)-*N*'-4-methoxybenzylidene)-5-methyl-*1H*-pyrazole-3-carbohydrazide (E-MBPC) in both media with the corresponding experimental ones.

B3LYP/6-311++G** Method[a]			Experimental[a]
Parameters	Gas	PCM	
Bond lengths (Å)			
N16-C17	1.280	1.285	1.278(3)
N16-N18	1.356	1.369	1.384(19)
N18-C20	1.391	1.361	1.344(2)
C20=O21	1.208	1.236	1.231(19)
C20-C22	1.495	1.482	1.477(2)
C22-N28	1.330	1.338	1.331(2)
N24-N28	1.343	1.341	1.344(2)
N24-C25	1.362	1.360	1.345(3)
C23-C25	1.380	1.382	1.370(2)
C25-C29	1.494	1.490	1.496(3)
C22-C23	1.421	1.416	1.392(3)
C17-C2	1.460	1.456	1.454(2)
RMSD	**0.021**	**0.012**	
Bond angles (º)			
C2-C17-N16	122.2	122.6	123.7(15)
C17-N16-N18	117.3	115.5	114.5(14)
N16-N18-C20	121.3	121.2	120.3(13)
N18-C20-O21	123.9	122.9	123.1(15)
C22-C20-O21	124.1	122.5	122.2(17)
C20-C22-N28	119.5	118.6	120.3(16)
C20-C22-C23	129.2	130.2	127.8(14)
C22-N28-N24	104.3	104.3	103.6(15)
N28-N24-C25	114.0	113.8	113.6(13)
N24-C25-C29	122.9	122.6	121.8(15)
N24-C25-C23	105.0	105.4	105.6(16)
C8-C7-O1	115.6	115.6	115.1(19)
C7-O1-C11	118.7	118.6	118.1(18)
RMSD	**1.3**	**1.0**	
Dihedral angles (º)			
C2-C17-N16-N18	-179.2	-179.5	-179.3(14)
C17-N16-N18-C20	-174.2	-178.7	-179.3(14)
N16-N18-C20-O21	2.4	2.7	-1.6(3)
N16-N18-C20-C22	-176.8	-177.2	178.0(13)
N18-C20-C22-N28	-149.7	-167.4	-4.2(2)
N18-C20-C22-C23	31.6	13.2	177.9(16)
O21-C20-C22-N28	30.9	12.6	175.4(16)
C20-C22-N28-N24	-178.9	-179.6	-178.4(14)
RMSD	**153.9**	**160.6**	

[a] This work, RMSD values in bold letters.

3.3. Geometrical parameters

In Table 4 are summarized the optimized geometrical parameters of (*E*)-*N*'-4-methoxybenzylidene)-5-methyl-*1H*-pyrazole-3-carbohydrazide (**E-MBPC)** in gas phase and aqueous solution by using the B3LYP/6-311++G** method. These parameters are compared in the same table with the corresponding experimental ones determined in this work by using the Root-mean-square deviation (RMSD) values. The exhaustive analysis shows that better correlations are observed for **E-MBPC** in solution, with RMSD values around 0.021 and 0.012 Å for bond lengths and of 1.3 and 1.0º for bond angles. Here, newly as observed in a similar previously studied derivative [55], the dihedral angles related to hydrazonoic group present the higher variations. In **E-MBPC**, the B3LYP/6-311++G** calculations predict higher values in gas phase (153.9º), as compared with those predicted in aqueous solution

(160.6 º). The dihedral N16-N18-C20-O21 and N16-N18-C20-C22 angles have signs different from the experimental ones while the other N18-C20-C22-N28, N18-C20-C22-C23 and O21-C20-C22-N28 angles present the same signs but values different from the experimental ones. Here, the differences observed between theoretical and experimental results can be attributed to the calculations because these were performed in the gas phase where the packing forces of solid state were not considered. These comparisons have demonstrated that despite of differences observed in the dihedral angles both optimized structures by using the B3LYP/6-311++G** method can be used to obtain the force fields of **E-MBPC** in both media due to the predicted low RMSD values of bond lengths and angles.

3.4. NBO and AIM analyses

The Second Order Perturbation Theory Analysis of Fock Matrix in NBO Basis is an interesting calculation used to know different types of interactions when there are acceptors and donors groups present in a species, as in **E-MBPC,** by using the version 3.1 of NBO program [46]. On the other hand, the topological properties allow evaluating different types of interactions such as, inter- or intramolecular, ionic or of Hydrogen bonds interactions based in the Bader's theory of atoms in molecules (AIM) and by using the version 2000 of AIM program [47,48]. Hence, with these two types of calculations it is possible predict the stabilities of **E-MBPC** in the two studied media. In the NBO study, the main delocalization energies for **E-MBPC** in gas phase and aqueous solution by using the B3LYP/6-311++G** method are presented in Table S2. The deep evaluation of that table shows the presence in **E-MBPC** of five interactions in solution but only four in gas phase. The former interactions observed in solution are: the $\Delta E_{\pi\rightarrow\pi^*}$, $\Delta E_{n\rightarrow\pi*}$, $\Delta E_{n\rightarrow\sigma^*}$, $\Delta E_{\sigma\rightarrow\sigma*}$ and $\Delta E_{\pi^*\rightarrow\pi^*}$ interactions while the $\Delta E_{\sigma\rightarrow\sigma*}$ interaction is not observed in gas phase. Consequently, the $\Delta E_{\pi^*\rightarrow\pi^*}$ interactions show the highest energy values in both media with a value of 2073.24 kJ/mol in solution and of 1879.54 kJ/mol in gas phase. The total energy of 4435.61 kJ/mol favours to **E-MBPC** in solution suggesting its higher stability in this medium, as also was observed for the (*E*)-*N'*-(4-(dimethylamino)benzylidene)-5-methyl-*1H*-pyrazole-3-carbohydrazide derivative in solution [55].

Here, the topological properties, which are, the electron density, $\rho(r)$, the Laplacian values, $\nabla^2\rho(r)$, the eigenvalues ($\lambda1$, $\lambda2$, $\lambda3$) of the Hessian matrix and, the $|\lambda1|/\lambda3$ ratio calculated for **E-MBPC** in both media in the Ring critical point (RCPs) are presented in Table S3. The values of properties only show changes in the R2 ring in solution, as compared with the corresponding in gas phase while the properties of R2 rings in both media are higher than the observed for R2. Note that these properties are not presented in the Bond Critical Points (BCPs) because from this study are not observed intra-molecular, ionic or of Hydrogen bonds interactions. For these reasons, only the RCP1 and RCP2 of both R1 and R2 rings respectively are presented in Table S3 while the molecular graphic of **E-MBPC** in gas phase is given in Fig. S5. The figure shows clearly the two RCP1 and RCP2 and the BCPs of existent bonds while new bonds are not formed.

3.5. Vibrational study

The experimental FT-IR spectrum of **E-MBPC** in the solid state can be seen in Fig. 5 compared with the corresponding predicted in the gas phase by using the B3LYP/6-311++G** method. Reasonable correlation was observed between both spectra because a higher number of bands were experimentally observed in the lower wavenumbers region, as compared with the theoretical one. These differences can be justified by the calculations which were performed in the gas phase where the interactions due to crystalline packing were not considered. For the same reasons, in the higher wavenumber (4000–2000 cm^{-1}) region the band attributed to N–H stretching modes is predicted at higher wavenumbers different from the observed in the experimental spectrum. The predicted Raman spectrum of **E-MBPC** in the gas phase is shown in Fig. S6 while in Fig. S7 can be seen comparisons between the predicted IR spectra of **E-MBPC** in both media by using the B3LYP/6-311++G** level of theory. Strong changes in the intensities and positions of the bands related to N–H groups are observed in the predicted IR spectrum in solution as a consequence of hydration process. The theoretical Raman spectrum predicted in activities was corrected to intensities by using known equations [53]. The N16=C17, C3=C5 and C8=C10 stretching modes are predicted with higher intensities in the Raman spectrum while in the infrared spectrum only the C3=C5 and C8=C10 stretching modes are predicted most intense than the other ones. According to the total number of atoms (33) present in the structure of **E-MBPC** a total of 93 vibration modes are expected in both media and, where all of them present activity in both spectra because the structures were optimized in the two media with symmetries C_1. The SQMFF methodology with the Molvib program were used to compute the force fields of **E-MBPC** in both media at the same level of theory while transferable scaling factors together with the normal internal coordinates and the experimental IR spectrum were employed to perform the complete vibrational assignments [50–52]. Only Potential energy distribution contributions (PED) $\geq$ 10% were considered in the assignments of vibration modes. Observed and calculated wavenumbers and assignments for **E-MBPC** in gas phase by using the B3LYP/6-311++G** method are shown in Table 5. After that, a brief discussion of assignments by regions is presented at continuation.

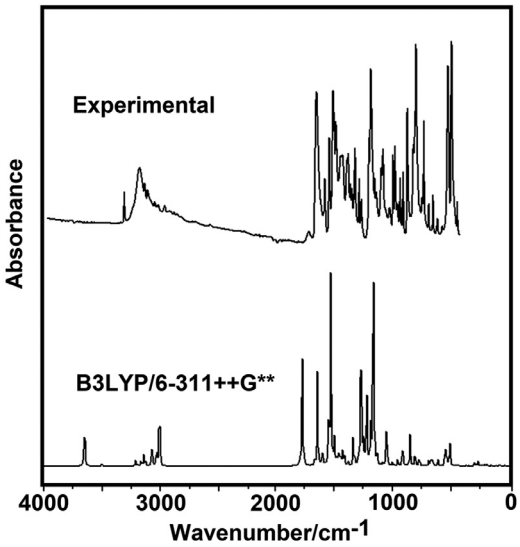

Fig. 5. Experimental infrared spectrum of (*E*)-*N'*-(4-methoxybenzylidene)-5-methyl-*1H*-pyrazole-3-carbohydrazide (**E-MBPC**) compared with the corresponding predicted for the free base by using B3LYP/6-311++G** level of theory.

Assignments bands: 4000–2000 cm^{-1} region. In this region, the stretching modes of N–H, C–H and CH_3 groups present in **E-MBPC** are expected. The bands characteristics of NH groups are generally observed around 3500–3300 cm^{-1} [55,59]. This absorption is strongly influenced by the chemical environment, in particular when NH groups are involved in the intramolecular or intermolecular hydrogen bond [55,60]. The NH stretching vibrations for pyrazole are reported at 3142 cm^{-1} by Altürk et al. [61] and at 3201 cm^{-1} by Sundaraganesan et al. [62]. González-Baró et al.

Table 5
Observed and calculated wavenumbers (cm^{-1}) and assignments for (*E*)-*N*'-4-methoxybenzylidene)-5-methyl-*1H*-pyrazole-3-carbohydrazide (**E-MBPC)** in gas phase by using the B3LYP/6-311++G** method.

(*E*)-*N*'-4-methoxybenzylidene)-5-methyl-*1H*-pyrazole-3-carbohydrazide				
Experimental[a]	B3LYP/6-311++G** Method[a]			
ATR	Calculated[b]	Intensity[c]	SQM[d]	Assignments[a]
3322 w	3644	110.6	3494	νN24-H27
3322 w	3493	6.9	3348	νN18-H19
3188m	3245	0.6	3111	νC23-H26
3152m	3206	12.6	3073	νC5-H6
3116w	3202	2.7	3070	νC10-H15
3060w	3187	2.5	3055	νC8-H9
3025w	3158	12.4	3027	νC3-H4
	3135	23.2	3006	ν_aCH$_3$(C11)
2971w	3120	8.1	2991	ν_aCH$_3$(C29)
2932w	3074	12.4	2947	ν_aCH$_3$(C29)
2932w	3065	36.6	2939	ν_aCH$_3$(C11)
	3027	35.1	2902	ν_sCH$_3$(C29)
2897w	3006	72.9	2882	ν_sCH$_3$(C11)
2897w	2999	63.7	2875	νC17-H33
1675s	1779	348.3	1714	νC20=O21
1606m	1672	7.1	1612	νC17=N16
1568m	1647	190.2	1595	νC8-C10νC3-C5
1532s	1609	12.9	1556	νC23-C25
1532s	1603	23.7	1552	νC5-C7
1509s	1554	94.0	1510	βN18-H19
1509s	1534	472.4	1488	βN18-H19βC10-H15
1464m	1506	0.6	1448	δ_aCH$_3$(C29)νC25-N24
1453m	1505	54.5	1442	δ_aCH$_3$(C11)
1444sh	1493	9.6	1428	δ_aCH$_3$(C11)
1420sh	1484	8.1	1421	δ_aCH$_3$(C29)
1420sh	1475	15.3	1419	νC22-N28νC22-C20
1405m	1465	21.8	1411	δ_sCH$_3$(C11)
1405m	1451	27.3	1407	νC8-C10νC3-C5
1385sh	1438	5.9	1394	νC22-N28
1365w	1430	34.4	1376	νC22-C23
1349m	1415	17.8	1355	δ_sCH$_3$(C29)
1313w	1386	10.5	1347	βC17-H33
1285w	1342	65.7	1298	βC3-H4νC5-C7
1285w	1329	10.4	1295	νC2-C3
1210vs	1296	12.1	1255	βN24-H27νC25-N24
1210vs	1275	365.3	1231	νC7-O1
1210vs	1254	50.4	1216	νC2-C17
1210vs	1226	202.5	1187	νC20-N18
1177sh	1202	11.2	1170	ρCH$_3$(C11)
1166sh	1192	72.1	1158	βC3-H4βC5-H6
1154sh	1170	482.6	1137	ρ'CH$_3$(C11)
1121w	1168	0.7	1130	νN24-N28
	1152	26.1	1118	βC23-H26
1106m	1134	19.6	1101	βC8-H9βC10-H15βC5-H6
1106m	1087	5.6	1054	νN18-N16
1024m	1062	1.5	1035	ρ'CH$_3$(C29)
1024m	1058	91.6	1024	βR$_1$(A2)
1024m	1045	9.0	1020	νC11-O1
1003m	1023	0.2	1000	βR$_1$(A1) νC7-C8
995sh	1007	7.3	985	βR$_2$(A2)
995sh	994	0.4	985	γC10-H15
967m	989	3.7	961	ρCH$_3$(C29)
955sh	960	12.7	952	γC17-H33
935m	929	2.3	921	γC3-H4
898s	916	51.9	903	βC20=O21
	855	34.3	844	γC8-H9
828vs	854	38.9	833	νC2-C10
	813	15.1	803	γC5-H6
804sh	811	20.7	801	γC23-H26
760m	781	5.7	766	γC20=O21γC23-H26
760m	773	16.8	760	γC20=O21
712w	732	0.2	711	τR$_1$(A1)
700sh	694	11.9	678	τR$_1$(A2)
676w	676	19.3	659	τR$_1$(A2) νC25-C29
637w	661	18.3	647	βR$_3$(A1)
638	651	1.4	641	τR$_2$(A2)
600w	615	13.2	607	βR$_2$(A1)
553vs	554	39.3	547	γN24-H27
537sh	540	27.5	526	γC7-O1γC2-C17
521vs	514	49.1	512	γN18-H19
505sh	508	20.8	502	δC7O1C11βC7-O1
473w	471	2.3	466	βC2-C17

(*continued on next page*)

Table 5 (*continued*)

(*E*)-*N*′-4-methoxybenzylidene)-5-methyl-*1H*-pyrazole-3-carbohydrazide				
Experimental[a]	B3LYP/6-311++G** Method[a]			
ATR	Calculated[b]	Intensity[c]	SQM[d]	Assignments[a]
	453	3.8	447	βC7-O1 δC7O1C11
	433	0.3	416	τR_2(A1)
	401	0.3	382	τR_1(A1)τN16-C17
	370	2.1	364	νC22-C20
	347	2.9	343	βC25-C29
	303	7.3	295	γC25-C29γC22-C20
	286	2.7	284	δC7O1C11βC7-O1
	272	10.3	255	τN16-C17
	242	2.7	222	τwCH_3(C11)
	216	3.6	208	τwCH_3(C11) τN18-C20
	195	2.8	189	βC7-O1 δC20N18N16
	188	3.3	177	τR_3(A1)
	158	2.8	152	τN16-N18γC22-C20
	116	1.9	107	τO1-C7
	95	1.3	94	δC22C20N18βC22-C20
	81	3.9	74	τO1-C7τN16-N18
	60	0.1	54	τwCH_3(C29)
	49	0.8	44	τC20-C22
	38	2.7	38	δN18N16C17 δC20N18N16δC2C17N16
	30	0.2	27	τN16-N18τC17-C2
	26	0.4	24	τN18-C20

Abbreviations: ν, stretching; β, deformation in the plane; γ, deformation out of plane; τ , torsion; β_R. deformation ring τ_R, torsion ring; ρ, rocking; τw, twisting; δ, deformation; a, antisymmetric; s, symmetric; (A_1), Ring 1; (A_2), Ring 2.

[a] This work.

[b] From B3LYP/6-311++G**.

[c] Intensities in KM/Mole; method.

[d] From scaled quantum mechanics force field.

[63] reported the NH stretching mode (ν_{NH}) of the hydrazonoic group at 3157 cm^{-1}. In this case, the SQM calculations predict the N24-H27 and N18-H19 stretching modes at 3494 and 3348 cm^{-1}, for which, the FT-IR band at 3322 cm^{-1} are assigned to those two stretching modes corresponding to vibrations for pyrazole and hydrazonoic group (CONH–*N*=CH–), respectively. A very important observation is that the N18-H19 stretching mode in the Raman spectrum is predicted with higher intensity than the other one.

Normally, in related compounds the C–H stretching vibrations of aromatic rings are assigned in the region 3200–3000 cm^{-1} [26–28,55,59]. For **E-MBPC**, the CH stretching modes were predict by calculations between 3111 and 3027 cm^{-1}, hence, the group of bands between 3188 and 3025 cm^{-1} and the weak IR band at 2897 cm^{-1} are assigned to those vibration modes. Here, the C23-H26 stretching mode corresponding to the pyrazole ring is in good agreement with the value reported for 3,5-dimethylpyrazole (3,5-DMP) [62] while the C17-H33 stretching mode corresponding to hydrazonoic group is predicted the SQM calculations at 2875 cm^{-1} and assigned accordingly. The absorption bands which appear between 3025 and 2897 cm^{-1} are assigned to the antisymmetric and symmetric stretching modes of CH_3 groups belonging to hydrazonoic and methoxy groups. The symmetries of stretching modes corresponding to the CH_3 groups were no attributed because the Raman spectrum was not recorded but the SQM calculations predicted the symmetric modes with higher intensities than the other ones.

2000–1000 cm^{-1} region. The C=O, C=C, C–C and C–N stretching modes, deformation and rocking modes of NH, CH and CH_3 groups and, some deformations of pyrazole and benzyl rings of **E-MBPC** are characteristics of this region. In particular, the C=O stretching mode is usually assigned free of other vibrations (1800–1600 cm^{-1}) [55,59]. Here, the $\nu_{C=O}$ stretching mode is predicted by calculation as a intense band at 1714 cm^{-1}, for which, is assigned to the strong IR band at 1675 cm^{-1}. For hydrazonoic groups, that vibration mode was assigned at 1655 cm^{-1} by Sheeja et al. [64] and at 1656 cm^{-1} by de Freitas et al. [60]. The C=N stretching vibrations are reported at 1604 and 1603 cm^{-1} by Galić et al. [65] for aroylhydrazones while in amide compound these C–N stretching modes are assigned to IR bands between 1364 and 1367 cm^{-1}. On the other hand, Sundaraganesan et al. [62] assign the C–N stretching in 3,5-DMP at 1327 cm^{-1}. For **E-MBPC**, the C17=N16 and C22-N28 stretching modes corresponding to hydrazonoic and pyrazole groups, respectively are predict with low intensities in the IR spectrum at 1612 and 1394 cm^{-1} and, hence, these modes are assigned at 1606 and 1385 cm^{-1}. Note that the C22-N28 stretching mode is also predicted coupled with the C22-C20 stretching mode, as observed in Table 5. The N–N stretching mode has been reported at 1156 cm^{-1} by de Freitas et al. [60], at 1118 cm^{-1} by Sheeja et al. [64] and at 1112 cm^{-1} by Arunagiri et al. [65]. For **E-MBPC**, the N24–N28 and N18–N16 vibration modes corresponding to pyrazole and hydrazonoic groups, respectively are predict with different intensities at 1130 and 1054 cm^{-1} and, for these reasons, they are assigned to the weak and medium intensity IR bands at 1106 and 1121 cm^{-1}, respectively. The aromatic C=C stretching modes appear as characteristics bands assigned usually in the region 1200–1650 cm^{-1} [26–28,55,62]. For **E-MBPC**, the series of IR bands observed at 1568, 1532, 1405, 1365, 1285 and 1210 cm^{-1} can be easily assigned to the C=C and C–C stretching modes of phenyl and pyrazole rings, where clearly the bands at higher wavenumbers have double bonds characters while the remain ones have partial double bonds characters. The NH in-plane deformation vibration is reported [62] at 1266 cm^{-1} in 3,5-DMP and at 1210 cm^{-1} in hydrazonoic group [64]. In this case, the βN18-H19 vibration mode corresponding to pyrazole ring is predicted with great intensity at 1488 cm^{-1} while the βN24-H27 in-plane deformation mode of hydrazonoic group is predicted with low intensity at 1255 cm^{-1} and, both are predicted coupled with other vibration modes. Hence, the intense IR bands at 1509 and 1210 cm^{-1} are assigned to those two vibration modes. The C–H in-plane deformation vibrations are observed in the region

1300–1000cm^{-1} and are usually of medium to weak intensity [26–28,55,66]. Here, some bands due to C–H in-plane bending vibrations are coupled with other vibrations and they can be assigned to the bands in the region between 1509 and 1106 cm^{-1} because the SQM calculations predict those modes in this region. The C7-O1 and C11-O1 stretching modes are predicted at 1231 and 1020 cm^{-1} for which they are assigned respectively to the strong of medium intensity IR bands at 1210 and 1024 cm^{-1}.

1000–10 cm^{-1} region. In this region, the C–C and C–N stretching modes, C–H and N–H out-of-plane deformations, deformations, wagging and twisting modes of C=O group, twisting CH_3 and deformations and torsions modes of both pyrazole and 4-methoxybenzyl rings of **E-MBPC** are expected. In the (*E*)-*N*′-(4-(dimethylamino)benzylidene)-5-methyl-*1H*-pyrazole-3-carbohydrazide derivative, the C=O in-plane (βC=O) and out-of-plane (γC=O) deformations are assigned to 667 and 360 cm^{-1}, respectively [55,67] while in this derivative **E-MBPC** the βC20=O21 and γC20=O21 modes are predicted at 903 and 760 cm^{-1}. Hence, the IR bands observed at 898 and 760 cm^{-1} are assigned to those vibration modes. Here, the change of $N(CH_3)_2$ group in the benzyl ring of (*E*)-*N*′-(4-(dimethylamino)benzylidene)-5-methyl-*1H*-pyrazole-3-carbohydrazide by methoxy group in **E-MBPC** evidently has influence on those two vibration modes.

The out-of-plane CH deformations are predicted and assigned between 1100 and 600 cm^{-1} [26–28,55]. In this case, the IR bands between 1024 and 760 cm^{-1} are assigned to those vibration modes, as detailed in Table 5. On the other hand, the out-of-plane N24-H27 and N18-H19 deformations are predicted practically with the same intensity, hence, the strong IR bands at 553 and 521 cm^{-1}, respectively are assigned to those two deformation modes.

The deformation and torsion modes of pyrazole and benzyl rings are predicted in approximately the expected regions [26–28,55]. Here, in **E-MBPC** the three deformations of benzyl ring βR_1(A1), βR_2(A1) and βR_3(A1) are predicted at 1000, 607 and 647 cm^{-1} respectively while the torsion modes τR_1(A1), τR_2(A1) and τR_3(A1) at 711, 416 and 177 cm^{-1}. The two deformation modes of pyrazole βR_1(A2) and βR_2(A2) are predicted at 1024 and 985 cm^{-1} while the corresponding torsion modes τR_1(A2) and τR_2(A2) at 678 and 641 cm^{-1}. Therefore, these vibration modes only were assigned until 473 cm^{-1} because the IR spectrum was recorded up to 400 cm^{-1}. For the same reason, remain modes were predicted as observed in Table 5 but not assigned.

3.6. Force fields

Scaled internal force constants for **E-MBPC** in gas phase and aqueous solution were calculated from the corresponding harmonic force fields by using the B3LYP/6-311++G** method with the SQM methodology and the Molvib program [50–52]. These parameters are presented in Table 6 compared with the predicted for the free base and cationic species of (*E*)-*N*′-(4-(dimethylamino)benzylidene)-5-methyl-*1H*-pyrazole-3-carbohydrazide derivative at the same level of theory. Comparing first the force constants for **E-MBPC** in both media, it is clearly observed the variations in the values of $f(\nu C{=}O)$, $f(\nu C{-}N)_{Chain}$, $(\nu C{-}N)_R$ and $f(\nu N{-}N)_{Chain}$ force constants as a consequence of hydration of these involved groups in aqueous solution. In general, the values decrease in solution but in the $f(\nu N{-}N)_{Chain}$ force constant, a slight increase is observed because the N18-H19 bond that belong to N16-N18 bond of hydrazonoic group is probably hydrated and, hence, it produces a weakening of the other N16-N18 bond. When these force constants are compared with the other derivative [55] changes in some values are observed although other remains practically constants. Thus, the $f(\nu C = O)$, $f(\nu C{-}N)_{Chain}$, $f(\nu N{-}N)_{Chain}$ and $f(\nu C = C)_{R1}$ force constants in **E-MBPC** change because, as observed from vibrational study, the change of $N(CH_3)_2$ group in the benzyl ring of (*E*)-*N*′-(4-(dimethylamino)benzylidene)-5-methyl-*1H*-pyrazole-3-carbohydrazide by methoxy group has influence on the involved bonds.

3.7. NMR studies

The experimental ^{1}H and ^{13}C NMR spectra of **E-MBPC** were obtained by using TMS as an internal standard and DMSO-d_6 as solvent (Figs. S8 and S9). The ^{1}H NMR spectrum of the title molecule displayed a two singlets at δ = 2.25 and 2.93 ppm due to CH_3 (H30, H31 and H32) and OCH_3 (H12, H13 and H14) protons, respectively. The chemical shifts H26 of pyrazole proton appear as a singlet at δ = 6.47 ppm. The chemical shifts of the phenyl protons (H6 & H9) and (H4 & H15) appeared as two doublets at δ = 6.98 and 7.60 ppm, respectively. The chemical shifts of H33 of the azomethine (*N*=CH) and H19 of amide (NHCO) groups appear as a singlet at 8.39 and 11.44 ppm, respectively. The chemical shifts H27 of NH pyrazole appeared as singlet at δ = 13.05 ppm. The ^{13}C NMR spectra of the title compound showed the chemical shifts C7 and C20 for C–OCH_3 and C=O carbons are at 161.13 and 158.72 ppm, respectively. The signals at 146.52 ppm are clearly assigned for C17 of azomethine group (*N*=CH). The signals at 105.22, 140.45 and 147.53 ppm are assigned for C23, C25 and C22 of pyrazole carbons, while that the aromatic carbon (C2, C3, C5, C8 and C10) chemical shifts of **E-MBPC** occurred in the range of 114.76–129.02 ppm. On the other hand, the predicted ^{1}H and ^{13}C- chemical shifts for **E-MBPC** in gas phase and in aqueous solution by using the GIAO/B3LYP/6-311++G** method using as Ref. to TMS are shown in Tables 7 and 8, respectively compared with the corresponding experimental ones [54]. Better correlations are obtained for the H atoms (1.5–1.4 ppm) in solution than the C atoms (7.0–6.60 ppm), as observed from the RMSD values.

3.8. Frontier orbitals and descriptors of reactivity

E-MBPC has evidenced remarkable antioxidant and antidiabetic activities, as was also observed in another (*E*)-*N*′-(4-(dimethylamino)benzylidene)-5-methyl-*1H*-pyrazole-3-carbohydrazide derivative [55], and for this reason, the predictions of its reactivities and behaviours in both media are necessary to explain those observed biological properties. Hence, the frontier orbitals, its differences expressed as gap and the chemical potential (μ), electronegativity (χ), global hardness (η), global softness (S), global electrophilicity index (ω) and nucleophilicity indexes (E) descriptors were calculated in both media by using the B3LYP/6-311++G** level of theory [24,26–28,55]. These parameters in both media are presented in Table S4 compared with those calculated for the free base and cationic species of (*E*)-*N*′-(4-(dimethylamino)benzylidene)-5-methyl-*1H*-pyrazole-3-carbohydrazide at the same level of theory. When are compared the gap values for **E-MBPC** in both media a slight decrease is observed in the gap value in solution, as compared with the value in gas phase while when the two values are compared with the corresponding to (*E*)-*N*′-(4-(dimethylamino)benzylidene)-5-methyl-*1H*-pyrazole-3-carbohydrazide derivative higher gap values are observed for **E-MBPC** in both media. Hence, the two species of other derivative are most reactive than **E-MBPC** in both media. Evidently, the presence of $N(CH_3)_2$ group in the benzyl ring in the (*E*)-*N*′-(4-(dimethylamino)benzylidene)-5-methyl-*1H*-pyrazole-3-carbohydrazide increase the reactivity of this derivative, as compared with **E-MBPC**. Hence, the methoxy group incorporate to benzyl ring instead of $N(CH_3)_2$ group decrease the reactivity of **E-MBPC**. Probably, these results for **E-MBPC** justify its lower antioxidant activity against to (*E*)-*N*′-(4-(dimethylamino)benzylidene)-5-methyl-*1H*-pyrazole-3-carbohydrazide.

Table 6
Scaled internal force constants for (*E*)-*N*'-4-methoxybenzylidene)-5-methyl-*1H*-pyrazole-3-carbohydrazide (**E-MBPC)** in gas phase by using the B3LYP/6-311++G** method.

Force constants	(*E*)-*N*'-4-methoxybenzylidene)-5-methyl-*1H*-pyrazole-3-carbohydrazide		(*E*)-*N*'-(4-(dimethylamino)benzylidene)-5-methyl-*1H*-pyrazole-3-carbohydrazide[b]	
	Gas	PCM	Gas Phase	
			Free base	Cationic
$f(\upsilon N\text{-}H)$	6.50	6.45	6.49	5.72
$f(\upsilon C{=}O)$	11.76	9.62	11.69	9.15
$f(\upsilon C\text{-}H)_{R1}$	5.13	5.15	5.13	5.10
$f(\upsilon C\text{-}H)_{R2}$	5.29	5.32	5.29	5.10
$f(\upsilon C\text{-}N)_{Chain}$	9.46	9.27	7.46	6.10
$f(\upsilon C\text{-}N)_{R}$	6.74	6.61	6.74	4.32
$f(\upsilon N\text{-}N)_{R}$	5.86	5.97	5.85	3.90
$f(\upsilon N\text{-}N)_{Chain}$	5.64	5.31	5.56	6.73
$f(\upsilon C{=}C)_{R1}$	6.31	6.27	6.24	6.15
$f(\upsilon C{=}C)_{R2}$	6.84	6.80	6.84	7.31
$f(\upsilon CH_3)$	4.79	4.85	4.75	4.62
$f(\delta CH_3)$	0.54	0.53	0.55	0.55

Units are mdyn $Å^{-1}$ for stretching and mdyn Å rad^{-2} for angle deformations.
[a]This work.
[b]From Ref [55].

Table 7
Observed and calculated ^{1}H chemical shifts (δ in ppm) for (*E*)-*N*'-4-methoxybenzylidene)-5-methyl-*1H*-pyrazole-3-carbohydrazide (**E-MBPC)** in gas phase and in aqueous solution.

H atom	6-311++G**		Exp[a]
	Gas	PCM	
4-H	7.14	7.14	7.60
6-H	6.60	6.64	6.98
9-H	7.17	7.24	6.98
12-H	3.61	3.66	3.77
13-H	4.01	4.04	3.77
14-H	3.56	3.57	3.77
15-H	8.60	8.55	7.60
19-H	7.95	8.10	11.44
26-H	6.08	5.98	6.47
27-H	9.04	9.19	13.05
30-H	2.27	2.24	2.26
31-H	2.29	2.28	2.26
32-H	2.20	2.23	2.26
33-H	7.61	7.71	8.39
RMSD	**1.50**	**1.40**	

[a] This work GIAO/B3LYP/6-311++G** Ref. to TMS.

Table 8
Observed and calculated ^{13}C chemical shifts (δ in ppm) for (*E*)-*N*'-4-methoxybenzylidene)-5-methyl-*1H*-pyrazole-3-carbohydrazide (**E-MBPC**) in gas phase and aqueous solution by using the B3LYP/6-311++G** method.

C atoms	6-311++G**		Exp[a]
	Gas	PCM	
2-C	133.43	132.98	129.02
3-C	134.98	136.14	144.76
5-C	110.29	110.63	127.55
7-C	168.02	168.75	161.13
8-C	123.82	124.25	127.55
10-C	133.06	133.28	144.76
11-C	54.90	56.27	55.74
17-C	143.24	147.39	146.45
20-C	158.89	160.70	158.72
22-C	154.44	152.17	147.53
23-C	106.94	104.39	105.11
25-C	143.29	143.13	140.45
29-C	10.40	10.33	10.80
RMSD	**7.00**	**6.60**	

[a] This work GIAO/B3LYP/6-311++G** Ref. to TMS.

3.9. Ultaviolet-visible spectra

The ultraviolet-visible spectrum of **E-MBPC** in aqueous solution was predicted in aqueous solution by using NStates=100 and the B3LYP/6-311++G** method with the Time-dependent DFT calculations (TD-DFT), as integrate in the Gaussian09 program [40]. In Fig. S10 is given the predicted electronic spectrum of **E-MBPC**. This spectrum shows an intense band at λ = 313 nm and a shoulder at c.a. λ = 250 nm. When the positions of bands observed in this derivative are compared with those reported for the (*E*)-*N*'-(4-(dimethylamino)benzylidene)-5-methyl-*1H*-pyrazole-3-carbohydrazide derivative in aqueous solution at the same level of theory (maximum at λ = 343. nm and shoulder at λ = 268 nm), we observed a shifting of bands in **E-MBPC** towards lower wavelength due to change in the benzyl ring of $N(CH_3)_2$ group by the methoxy group [55]. These bands can be assigned to $\pi \rightarrow \pi^*$ and $n \rightarrow \pi^*$ transitions due to the presence of C=C double bonds of both pyrazole and benzyl rings and to carbohydrazide group because NBO calculations predict these different transitions. Here, as in the (*E*)-*N*'-(4-(dimethylamino)benzylidene)–5-methyl-*1H*-pyrazole-3-carbohydrazide derivative, the shoulder in the predicted UV–vis spectrum could be attributed to the cationic form which is also expected in solution. These assignments are in agreement with other reported for similar species [68,69].

3.10. ESI-MS

The ESI-MS spectra show molecular ion peaks with *m/z* values 259.5 corresponding to the molecular weight $[M + H]^+$. The m/z value 281.3 corresponds to the sodiated molecular ion peak $[M+Na]^+$ (Fig. S11). These values are in good agreement with the proposed composition for the title molecule ($C_{13}H_{14}N_4O_2$).

3.11. Hirshfeld surface analysis

In this part, the Hirshfeld surface analysis of (*E*)-*N*'-4-methoxybenzylidene-5-methyl-1H-pyrazole-3-carbohydrazide (**E-MBPC**) compound was carried out to visualize the molecular quantify and various intra/intermolecular interactions from surface mapped analysis. In computations and evaluations in the program,

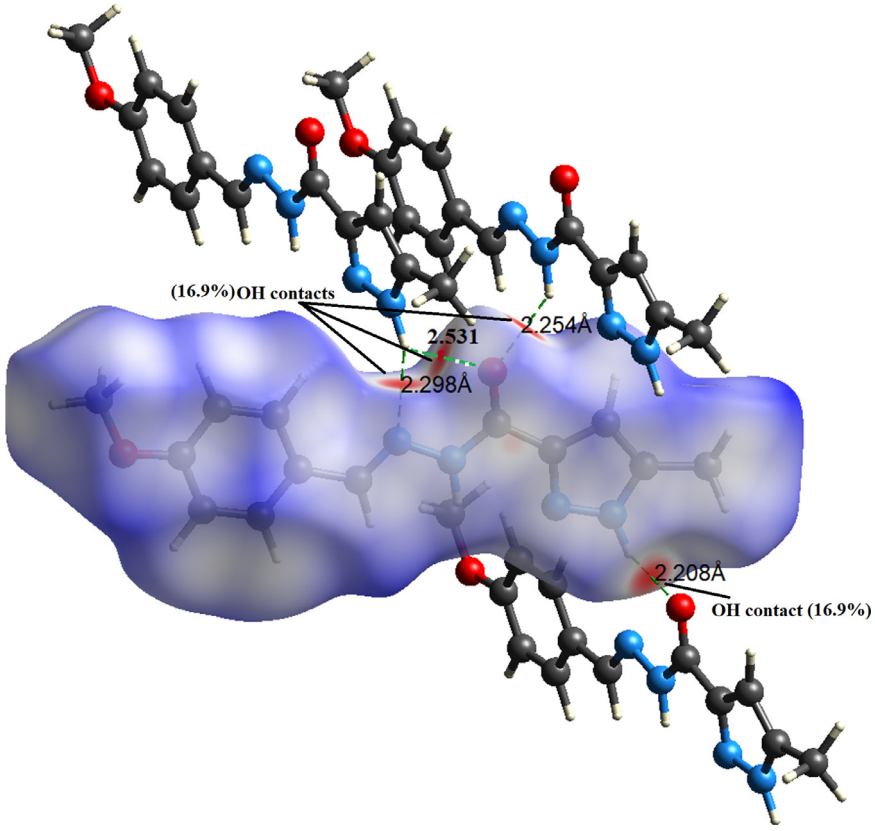

Fig. 6. d_{norm} mapped on Hirshfeld surface for visualizing the intercontacts of the title compound.

Crystallographic Information File (cif*) of the **E-MBPC** compound was used as an input file. When we look at Fig. 6 (d_{norm} mapped on Hirshfeld surface), we see that red, blue and white colors exist. Each of these colors corresponds to a type of interaction, in other words: short d_{norm} range for red and long d_{norm} range for blue [70,71]. Here, d_{norm} value was achieved as −0.3014: red points to 1.3880 a.u: blue colors and white color region with a dnorm value of zero. The dark red points near the O, N, H atoms result from N–H…N interactions with 2.298 Å (between pyrazole H and carbohydrazide N); N–H…O interactions with 2.531 Å (between pyrazole H and carbohydrazide O) and 2.254 Å (between carbohydrazide H and carbohydrazide O); C–O…H, interactions with 2.208 Å (between carbohydrazide O and pyrazole H) were observed.

The 2D fingerprint plot discloses that percentage (%) contribution to the Hirshfeld surface of each individual intermolecular contact as shown in the Fig. 7. According to this, the maximum and minimum contributions were obtained as H…H (44.4%), O…H/H…O and C···H/H···C (16.9%), N···H/H···N (11.6%) and N···C/C···N (6.3%), here the percentage contributions of other intermolecular contacts were less than 2% and not taken.

3.12. Molecular docking studies

Molecular docking has become an increasingly important method for both drug design and discovery, and has shed light on many experimental studies so far. In general molecular docking could be interpreted as computational estimation (their conformations and orientations) of protein and ligand complexes [72,73]. Endogenous cannabinoids (ECs) are lipid-signaling molecules that specifically bind to cannabinoid receptor types 1 and 2 (CB1R and CB2R) and are highly expressed in central and many peripheral tissues under pathological conditions. Activation of hepatic CB1R is associated with obesity, insulin resistance, and impaired metabolic function, owing to increased energy intake and storage, impaired glucose and lipid metabolism, and enhanced oxidative stress and inflammatory responses. Additionally, blocking peripheral CB1R improves insulin sensitivity and glucose metabolism and also reduces hepatic steatosis and body weight. Thus, targeting CB1R receptors may provide a potential therapeutic strategy against obesity and insulin resistance [74]. During our current research concerning the design and synthesis of novel antidiabetic compounds [18,55], we found that pyrazole derivatives possess an *in vivo* hypoglycemic effect due to its interactions with peripheral CB1R [75]. In present study, **E-MBPC** compound was prepared and optimized with B3LYP/6-311++G(d,p), and the optimized structure was converted into Protein Data Bank (PDB) format, then the pdbqt format of the **E-MBPC** ligand was recorded considering the tor-

Table 9
AutoDockVina results of the binding affinity and RMSD values of different poses in 4AMJ inhibitors of E-MBPC compound.

Modes	E-MBPC-4AMJ		
	Affinity(kcal/mol)	rmsdl.b.	rmsdu.b.
1	-8.5	0.000	0.000
2	-8.2	6.802	7.590
3	-7.1	2.613	8.532
4	-7.1	33.900	37.093
5	-6.9	29.741	33.519
6	-6.8	29.815	34.002
7	-6.7	33.893	36.950
8	-6.6	25.734	29.504
9	-6.4	33.063	36.808
10	-6.4	33.271	37.284
Inhibition Constant: 0.588105 μM			
Number of Hydrogen bonding: 4 active+1 non-active			

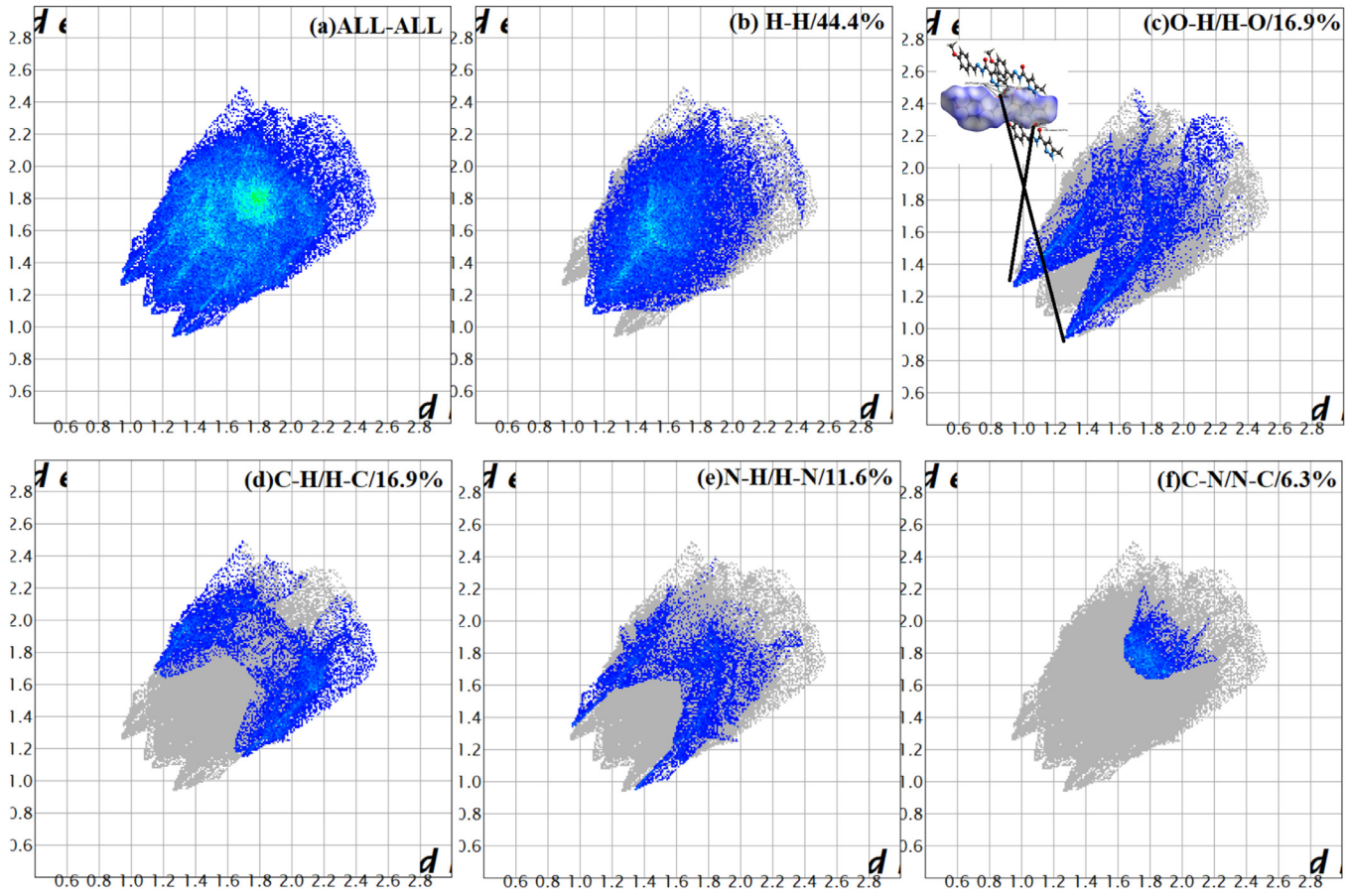

Fig. 7. Finger plots of the title compound.

sion dihedrals in the structure. In order to corroborate the possible mechanism of action of the title compound and understand the detailed ligand-receptor interactions, we carried out a molecular docking study in a CB1R. Such G protein-coupled receptor (GPCR) was modeled by using the B chain of β1-adrenergic receptor from M. gallopavo (PDB: 4AMJ, resolution of 2.30) target was retrieved in PDB format from protein data bank (PDB) [76] and all hetero atoms (co-factors) and water molecules were removed. During this analysis, the obtained docking results were described as follows:

The active sites of PDB: 4AMJ were fixed as TYR333, ASN329, PHE315, ASN310, LEU308, PHE307, PHE306, TRP303, MET296, LEU289, HIS286, TYR231, SER215, SER211, TYR207, ARG205, ASN204, PHE201, ASP200, CYS198, ASP195, TYR193, CYS192, TRP181, HIS180, PRO176, TRP166, THR164, ILE161, VAL160, ARG157, MET153, ASP121, TRP117 and LEU101. Later docking grid parameters were determined by taking into consideration the regions where active residues are concentrated as follows: center_x = 10.397, center_y=−8.579, center_z = 25.227, size_x = 64, size_y = 54, size_z = 74, spacing=0.531. The obtained docking scores and some important scales were given in Table 9 and Fig. 8. As seen from the Table 9, the best binding mode was determined with −8.5 (kcal/mol) energy and active four+one non-active hy-

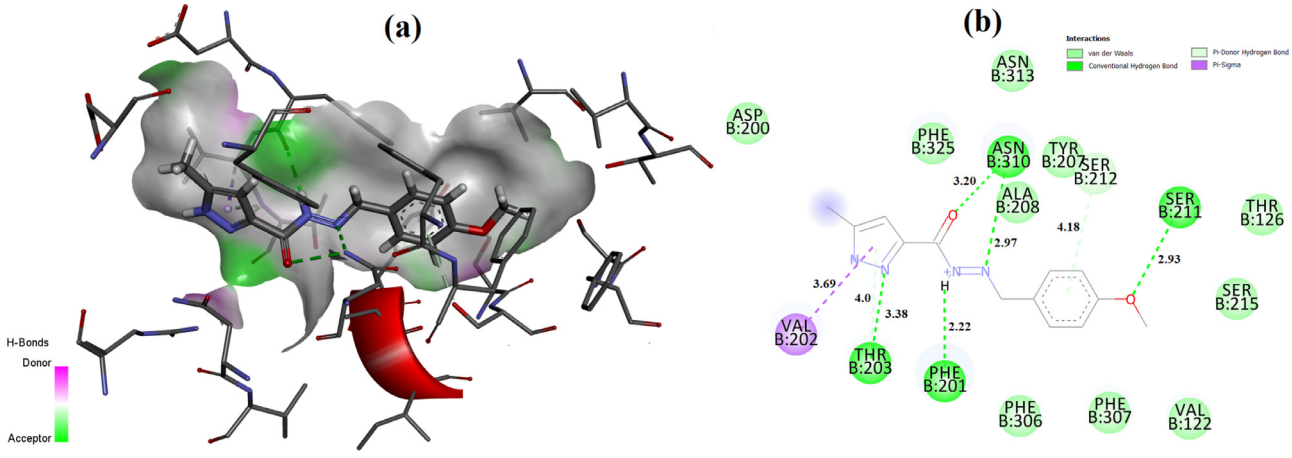

Fig. 8. The molecular docking results of the **E-MBPC** compound with 4AMJ protein, surfaces around ligand (a) and 2D forms (b).

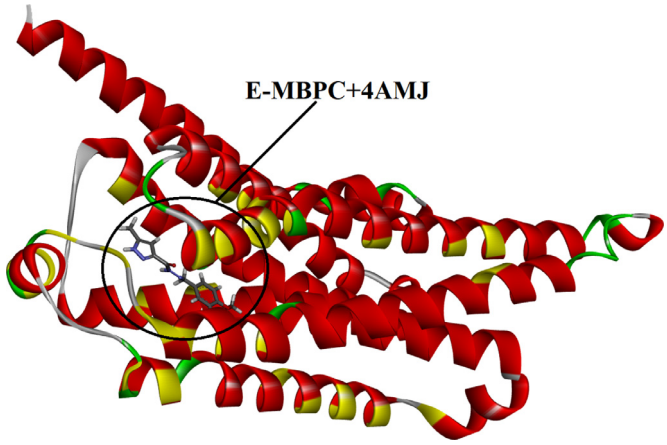

Fig. 9. The molecular docking positions of the **E-MBPC** compound with 4AMJ protein.

drogen bonding. These active hydrogen bondings were seen between ASN310 and O21 atom with 3.20 Å bond distance, ASN310 and N16 atom with 2.97 Å bond distance, PHE201 and H19 atom with 2.22 Å bond distance, SER211 and O1 atom with 2.93 Å bond distance; and non-active THR203 and N28 atom with 3.38 Å bond distance. Additionally van der Waals, π-donor hydrogen bond and π-sigma interactions and occurred bond distances were shown in Fig. 8 and position (the best binding mode) of ligand in protein: 4AMJ was shown in Fig. 9. Additionally, the inhibition constants for **E-MBPC** and PDB: 4AMJ were computed as 0.588105 μM with the help of K_i=exp(ΔG/RT) equation, where, ΔG, R and T are the docking binding energy, gas constant (1.9872036×10^{-3} kcal/mol) and room temperature (298.15 K), respectively. From the results it is concluded that (*E*)-*N'*−4-methoxybenzylidene-5-methyl-*1H*-pyrazole-3-carbohydrazide (E-MBPC) compound can be designed as potential antidiabetic agent.

4. Conclusions

In the present work, the (*E*)-*N'*-4-methoxybenzylidene-5-methyl-*1H*-pyrazole-3-carbohydrazide derivative (**E-MBPC**) was synthesized and characterized by using the FT-IR, ^{1}H & ^{13}C NMR and ESI-MS spectroscopic methods and, then, the (*E*)-configuration of hydrazonoic group was confirmed by single-crystal X-ray diffraction. The theoretical structures of **E-MBPC** in both media were determined in gas phase and aqueous solution by using the hybrid B3LYP/6-311++G** method. Calculations in solution were performed with SCRF method and the IEFPCM and universal solvation models. The resulted have shown that dipole moment increases from 7.97 D in gas phase to 13.68 D in solution with a slight contraction in the volume with a solvation energy of −131.34 kJ/mol. The three types of charges studied have evidenced that the protonation in solution could occur only in the N28 atom because these charges on these atoms show negative values while the three charges predict that both O atoms could be protonated in solution. The mapped MEP surfaces show that the nucleophilic region is wide and is located on the O21 and N28 atoms including the N16 atom while two clear electrophilic sites are observed on the N24-H27 and N18-H19 bonds. NBO calculations support the high stability of **E-MBPC** in solution. The frontier orbitals studies suggest low reactivity in both media, as compared with the (*E*)-*N'*-(4-(dimethylamino)benzylidene)-5-methyl-*1H*-pyrazole-3-carbohydrazide derivative. The vibrational assignments of 93 vibration modes expected for **E-MBPC** were reported together with the corresponding force fields and force constants in both media. The predicted Raman and Ultraviolet-visible spectra were also reported for **E-MBPC** at the same level of theory. Good correlations were obtained when the predicted ^{1}H- and ^{13}C-NMR spectra are compared with the corresponding experimental ones. On the basis of docking studies using 4AMJ protein, we can claim the importance of considering the title compound as a biological target for the generation of more potent antidiabetic agent.

Declaration of Competing Interest

None

CRediT authorship contribution statement

Khalid Karrouchi: Methodology, Writing - original draft, Writing - review & editing. **Silvia A. Brandán:** Software, Validation, Writing - review & editing. **Yusuf Sert:** Software, Writing - original draft. **Miloud El Karbane:** Resources. **Smaail Radi:** Supervision, Project administration. **Marilena Ferbinteanu:** Software, Validation, Writing - review & editing. **Yann Garcia:** Supervision, Investigation. **M'hammed Ansar:** Supervision, Project administration.

Acknowledgments

This work was supported by the WBI-COP22 Morocco project and UM5R as well as grants from CIUNT Project Nº 26/D608 (Consejo de Investigaciones, Universidad Nacional de Tucumán). The authors would like to thank Prof. Tom Sundius for his permission to use MOLVIB.

Supplementary materials

Supplementary material associated with this article can be found, in the online version, at doi:10.1016/j.molstruc.2020.129072.

References

[1] K. Karrouchi, S. Radi, Y. Ramli, J. Taoufik, Y. Mabkhot, F. Al-aizari, M. Ansar, Synthesis and pharmacological activities of pyrazole derivatives: a review, Molecules 23 (2018) 134.
[2] R.S. Padwal, S.R. Majumdar, Drug treatments for obesity: orlistat, sibutramine, and rimonabant, Lancet 369 (2007) 71–77.
[3] J.J. Cui, M. Tran-Dubé, H. Shen, M. Nambu, P.P. Kung, M. Pairish, M. McTigue, Structure based drug design of crizotinib (PF-02341066), a potent and selective dual inhibitor of mesenchymal–epithelial transition factor (c-MET) kinase and anaplastic lymphoma kinase (ALK), J. Med. Chem. 54 (2011) 6342–6363.
[4] N. Subramanian, S. Ray, S.K. Ghosal, R. Bhadra, S.P. Moulik, Formulation design of self-microemulsifying drug delivery systems for improved oral bioavailability of celecoxib, Biol. Pharm. Bull. 27 (2004) 1993–1999.
[5] S. Zisook, J. Mendels, D. Janowsky, J. Feighner, J.C. Lee, A. Fritz, Efficacy and safety of fezolamine in depressed patients, Neuropsychobiology 17 (1987) 133–138.
[6] E. Vinge, S. Björkman, Compared effects of the two antiinflammatory drugs indoprofen and lonazolac on thromboxane generation and on platelet aggregation, related to plasma concentrations after single oral doses, Acta Pharmacol. Toxicol. 59 (1986) 165–174.
[7] A. Charli, H. Jin, V. Anantharam, A. Kanthasamy, A.G. Kanthasamy, Alterations in mitochondrial dynamics induced by tebufenpyrad and pyridaben in a dopaminergic neuronal cell culture model, Neurotoxicology 53 (2016) 302–313.
[8] T.P. Selby, G.P. Lahm, T.M. Stevenson, K.A. Hughes, D. Cordova, I.B. Annan, T.F. Pahutski, Discovery of cyantraniliprole, a potent and selective anthranilic diamide ryanodine receptor activator with cross-spectrum insecticidal activity, Bioorg. Med. Chem. Lett. 23 (2013) 6341–6345.
[9] F.E. Bennani, L. Doudach, Y. Cherrah, Y. Ramli, K. Karrouchi, M. Ansar, M.E.A. Faouzi, Overview of recent developments of pyrazole derivatives as an anticancer agent in different cell line, Bioorg. Chem. (2019) 103470.
[10] K. Karrouchi, S. Fettach, S. Radi, J. Taoufik, Y.N. Mabkhot, S. Alterary, My E.A Faouzi, M. Ansar, Synthesis, characterization, free-radical scavenging capacity and antioxidant activity of novel series of hydrazone, 1, 3, 4-oxadiazole and 1, 2, 4-triazole derived from 3, 5-dimethyl-1H-pyrazole, Lett. Drug. Des. Discov. 16 (2019) 712–720.
[11] A. Titi, M. Messali, B.A. Alqurashy, R. Touzani, T. Shiga, H. Oshio, T.B Hadda, Synthesis, characterization, X-Ray crystal study and bioctivities of pyrazole derivatives: identification of antitumor, antifungal and antibacterial pharmacophore sites, J. Mol. Struct. 1205 (2020) 127625.

[12] K. Karrouchi, E.B. Yousfi, N.K. Sebbar, Y. Ramli, J. Taoufik, Y. Ouzidan, M. Ansar, Y.N. Mabkhot, H.A. Ghabbour, S. Radi, New pyrazole-hydrazone derivatives: x-ray analysis, molecular structure investigation via density functional theory (DFT) and their high in-situ catecholase activity, Int. J. Mol. Sci. 18 (2017) 2215.
[13] A.T. Taher, M.T.M. Sarg, N.R.E.S. Ali, N.H. Elnagdi, Design, synthesis, modeling studies and biological screening of novel pyrazole derivatives as potential analgesic and anti-inflammatory agents, Bioorg. Chem. 89 (2019) 103023.
[14] S. Tighadouini, R. Benabbes, M. Tillard, D. Eddike, K. Haboubi, K. Karrouchi, S. Radi, Synthesis, crystal structure, DFT studies and biological activity of (Z)-3-(3-bromophenyl)-1-(1, 5-dimethyl-1 H-pyrazol-3-yl)-3-hydroxyprop-2-en-1-one, Chem. Cent. J. 12 (1) (2018) 122.
[15] Y. Xu, Z. Zhang, X. Jiang, X. Chen, Z. Wang, H. Alsulami, W. Tang, Discovery of δ-sultone-fused pyrazoles for treating Alzheimer's disease: design, synthesis, biological evaluation and SAR studies, Eur. J. Med. Chem. 181 (2019) 111598.
[16] K. Karrouchi, L. Chemlal, J. Taoufik, Y. Cherrah, S. Radi, M.-.E. Faouzi, M. Ansar, Synthesis, antioxidant and analgesic activities of Schiff bases of 4-amino-1, 2, 4-triazole derivatives containing a pyrazole moiety, Ann. Pharm. Fr. 74 (2016) 431–438.
[17] K. Chkirate, S. Fettach, K. Karrouchi, N.K. Sebbar, E.M. Essassi, J.T. Mague, S. Radi, M.E.A. Faouzi, N.N. Adarsh, Garcia, Y. Novel Co (II) and Cu (II) coordination complexes constructed from pyrazole-acetamide: effect of hydrogen bonding on the self assembly process and antioxidant activity, J. Inorg. Biochem. 191 (2019) 21–28.
[18] R.R. Pillai, K. Karrouchi, S. Fettach, S. Armaković, S.J. Armaković, Y. Brik, J. Taoufik, S. Radi, M.E.A. Faouzi, M.H. Ansar, Synthesis, spectroscopic characterization, reactive properties by DFT calculations, molecular dynamics simulations and biological evaluation of Schiff bases tethered 1, 2, 4-triazole and pyrazole rings, J. Mol. Struct. 1177 (2019) 47–54.
[19] H. Dai, Y.-S. Xiao, Z. Li, X.-Y. Xu, X.-H. Qian. Dai, H. Xiao, Y.S. Li, Z. Xu, X. Y., X.H. Qian, The thiazoylmethoxy modification on pyrazole oximes: synthesis and insecticidal biological evaluation beyond acaricidal activity. Chinese Chemical Letters, Chin. Chem. Lett. 25 (7) (2014) 1014–1016.
[20] K. Korber, F. Kaiser, G. Veitch, W. Von Deyn, N.G. Bandur, J. Dickhaut, K. Gunjima. U.S. Patent No. 9,174,967. Washington, DC: U.S. Patent and Trademark Office (2015).
[21] Y.C Lang, Y.L. Bai, Research and development progresses on pyrazole agrochemicals., Mod. Agrochem. 5 (2006) 6.
[22] L.R.S. Dias, R.R.S. Salvador, Pyrazole carbohydrazide derivatives of pharmaceutical interest, Pharmaceuticals 5 (2012) 317–324.
[23] S. Rollas, S.G. Küçükgüzel, Biological activities of hydrazone derivatives, Molecules 12 (2007) 1910–1939.
[24] J. Kausteklis, V. Aleksa, M.A. Iramain, S.A. Brandán, Cation-anion interactions in 1-buthyl-3-methyl imidazolium nitrate ionic liquid and their effect on their structural and vibrational properties, J. Mol. Struct. 1164 (2018) 1–14.
[25] Y. Bouzian, K. Karrouchi, Y. Sert, C.H. Lai, L. Mahi, N.H. Ahabchane, A. Talbaoui, J.T. Mague, E.M. Essassi, Synthesis, spectroscopic characterization, crystal structure, DFT, molecular docking and in vitro antibacterial potential of novel quinoline derivatives, J. Mol. Struct 1209 (2020) 127940.
[26] O. Noureddine, S. Gatfaoui, S.A. Brandán, H. Marouani, N. Issaoui, Structural, docking and spectroscopic studies of a new piperazine derivative, 1-Phenylpiperazine-1,4-diium-bis (hydrogen sulfate), J. Mol. Struct. 1202 (2020) 127351.
[27] S. Gatfaoui, N. Issaoui, S.A. Brandán, T. Roisnel, H. Marouani, Synthesis and characterization of p-xylylenediaminiumbis(nitrate). Effects of the coordination modes of nitrate groups on their structural and vibrational properties, J. Mol. Struct. 1151 (2018) 152–168.
[28] O. Noureddine, S. Gatfaoui, S.A. Brandan, A. Sagaama, H. Marouani, N. Issaoui, Experimental and DFT studies on the molecular structure, spectroscopic properties, and molecular docking of 4-phenylpiperazine-1-ium dihydrogen phosphate, J Mol. Struct. 1207 (2020) 127762.
[29] K. Karrouchi, M. Ansar, S. Radi, M. Saadi, L. El Ammari, Crystal structure of N′-diphenylmethylidene-5-methyl-1H-pyrazole-3-carbohydrazide, Acta Cryst. E 71 (2015) o890–o891.
[30] K. Karrouchi, S. Radi, J. Taoufik, H.A. Ghabbour, Y.N. Mabkhot, Crystal structure of N′-(4-(dimethylamino) benzylidene)-5-phenyl-1H-pyrazole-3-carbohydrazide, C19H19N5O. Z. Kristallogr. NCS 231 (2016) 883–886.
[31] K. Karrouchi, S. Radi, J. Taoufik, H.A. Ghabbour, Y.N. Mabkhot, Crystal structure of N′-(4-methoxybenzylidene)-5-phenyl-1H-pyrazole-3-carbohydrazide, C18H16N4O2. Z. Kristallogr, NCS 231 (2016) 835–837.
[32] K. Karrouchi, S. Radi, J. Taoufik, H.A. Ghabbour, Y.N. Mabkhot, Crystal structure of N′-(4-nitrobenzylidene)-5-phenyl-1H-pyrazole-3-carbohydrazide, C17H13N5O3. Z. Kristallogr. NCS 231 (2016) 839–841.
[33] Crystal Structure 4.2: Crystal Structure Analysis Package, Rigaku Corporation (2000-2015). Tokyo 196–8666, Japan.
[34] O.V. Dolomanov, L.J. Bourhis, R.J. Gildea, J.A.K. Howard, H. Puschmann, OLEX2: a complete structure solution, refinement and analysis program, J. Appl. Cryst. 42 (2009) 339–341.
[35] G.M. Sheldrick, Acta Crystallogr., Sect. C 71 (2015) 3–8.
[36] C.F. Macrae, P.R. Edgington, P. McCabe, E. Pidcock, G.P. Shields, R. Taylor, M. Towler, J. Van De Streek, Mercury: visualization and analysis of crystal structures, J. Appl. Crystallogr. 39 (2006) 453–457.
[37] G.M. Sheldrick, Crystal structure refinement with SHELXL, Acta Cryst. C 71 (2015) 3–8.
[38] C. Lee, W. Yang, R.G. Parr, Development of the Colle-Salvetti correlation-energy formula into a functional of the electron density, Phys. Rev. B3 (1988) 785–789.
[39] A.D. Becke, Density-functional exchange-energy approximation with correct asymptotic behavior, Phys. Rev. A38 (1988) 3098–3100.
[40] Gaussian 09, Revision A.02, M.J. Frisch, G.W. Trucks, H.B. Schlegel, G.E. Scuseria, M.A. Robb, J.R. Cheeseman, G. Scalmani, V. Barone, B. Mennucci, G.A. Petersson, H. Nakatsuji, M. Caricato, X. Li, H.P. Hratchian, A.F. Izmaylov, J. Bloino, G. Zheng, J.L. Sonnenberg, M. Hada, M. Ehara, K. Toyota, R. Fukuda, J. Hasegawa, M. Ishida, T. Nakajima, Y. Honda, O. Kitao, H. Nakai, T. Vreven, J.A. Montgomery, Jr., J.E. Peralta, F. Ogliaro, M. Bearpark, J.J. Heyd, E. Brothers, K.N. Kudin, V.N. Staroverov, R. Kobayashi, J. Normand, K. Raghavachari, A. Rendell, J.C. Burant, S.S. Iyengar, J. Tomasi, M. Cossi, N. Rega, J.M. Millam, M. Klene, J.E. Knox, J.B. Cross, V. Bakken, C. Adamo, J. Jaramillo, R. Gomperts, R.E. Stratmann, O. Yazyev, A.J. Austin, R. Cammi, C. Pomelli, J.W. Ochterski, R.L. Martin, K. Morokuma, V.G. Zakrzewski, G.A. Voth, P. Salvador, J.J. Dannenberg, S. Dapprich, A.D. Daniels, Ö. Farkas, J.B. Foresman, J.V. Ortiz, J. Cioslowski, and D.J. Fox, Gaussian, Inc., Wallingford CT, 2009.
[41] S. Miertus, E. Scrocco, J. Tomasi, Electrostatic interaction of a solute with a continuum, Chem. Phys. 55 (1981) 117–129.
[42] J. Tomasi, J. Persico, Molecular interactions in solution: an overview of methods based on continous distributions of the solvent, Chem. Rev. 94 (1994) 2027–2094.
[43] A.V. Marenich, C.J. Cramer, D.G. Truhlar, Universal solvation model based on solute electron density and a continuum model of the solvent defined by the bulk dielectric constant and atomic surface tensions, J. Phys. Chem. B113 (2009) 6378–6396.
[44] P. Ugliengo, MOLDRAW Program, University of Torino, Dipartimento Chimica IFM, Torino, Italy, 1998.
[45] B.H. Besler, K.M. Merz Jr, P.A. Kollman, Atomic charges derived from demiempirical methods, J. Comp. Chem. 11 (1990) 431–439.
[46] E.D. Gledening, J.K. Badenhoop, A.D. Reed, J.E. Carpenter, F.F. Weinhold, NBO 3.1, Theoretical Chemistry Institute, University of Wisconsin, Madison, WI, 1996.
[47] R.F.W. Bader, Atoms in Molecules. A Quantum Theory, ISBN: 0198558651, Oxford University Press, Oxford, 1990.
[48] F. Biegler-Köning, J. Schönbohm, D. Bayles, AIM2000; A Program to Analyze and Visualize Atoms in Molecules, J. Comput. Chem. 22 (2001) 545.
[49] A.B. Nielsen, A.J. Holder, *GaussView*, Userś Reference, GAUSSIAN, Inc.: Pittsburgh, PA, USA, 2000–2003.
[50] P. Pulay, G. Fogarasi, G. Pongor, J.E. Boggs, A. Vargha, Combination of theoretical ab initio and experimental information to obtain reliable harmonic force constants. Scaled quantum mechanical (QM) force fields for glyoxal, acrolein, butadiene, formaldehyde, and ethylene, J. Am. Chem. Soc. 105 (1983) 7073.
[51] G. Rauhut, P. Pulay, Transferable scaling factors for density functional derived vibrational force fields, J. Phys. Chem. 99 (1995) 3093–3100.
[52] T. Sundius, Scaling of ab-initio force fields by MOLVIB, Vib. Spectrosc. 29 (2002) 89–95.
[53] G. Keresztury, S. Holly, G. Besenyei, J. Varga, A.Y. Wang, J.R. Durig, Vibrational spectra of monothiocarbamates-II. IR and Raman spectra, vibrational assignment, conformational analysis and ab initio calculations of S-methyl-N,N-dimethylthiocarbamate, Spectrochim. Acta 49A (1993) 2007–2026.
[54] R. Ditchfield, Self-consistent perturbation theory of diamagnetism. I. A gage-invariant LCAO (linear combination of atomic orbitals) method for NMR chemical shifts, Mol. Phys. 27 (1974) 714–722.
[55] K. Karrouchi, S.A. Brandán, Y. Sert, H. El-marzouqi, S. Radi, M. Ferbinteanu, M.E.A. Faouzi, Y. Garcia, M Ansar, Synthesis, X-ray structure, vibrational spectroscopy, DFT investigation and biological evaluation studies of (*E*)-*N*′ -(4-(dimethylamino)benzylidene)-5-methyl-*1H* -pyrazole-3-carbohydrazide, J. Mol. Struct. 128541 (2020).
[56] M. Turner, J. McKinnon, S. Wolff, D. Grimwood, P. Spackman, D. Jayatilaka, M. Spackman, CrystalExplorer17; University of Western Australia: crawley, WA, Australia, 2017, (2017).
[57] http://www.3dsbiovia.com/in.
[58] O. Trott, A.J. Olson, AutoDock Vina, improving the speed and accuracy of docking with a new scoring function, efficient optimization, and multithreading, J. Comput. Chem. 31 (2010) 455–461.
[59] P. Larkin, Infrared and Raman spectroscopy: Principles and Spectral Interpretation, Elsevier, 2017.
[60] L.V. de Freitas, C.C. da Silva, J. Ellena, L.A.S. Costa, N.A. Rey, Structural and vibrational study of 8-hydroxyquinoline-2-carboxaldehyde isonicotinoyl hydrazone–A potential metal–protein attenuating compound (MPAC) for the treatment of Alzheimer's disease, Spectrochim. Acta A.116 (2013) 41–48.
[61] S. Altürk, D. Avcı, Ö. Tamer, Y. Atalay, 1H–pyrazole–3–carboxylic acid: experimental and computational study, J. Mol. Struct. 1164 (2018) 28–36.
[62] N. Sundaraganesan, E. Kavitha, S. Sebastian, J.P. Cornard, M. Martel, Experimental FTIR, FT-IR (gas phase), FT-Raman and NMR spectra, hyperpolarizability studies and DFT calculations of 3, 5-dimethylpyrazole, Spectrochim. Acta. Part A. 74 (2009) 788–797.
[63] A.C. González-Baró, R. Pis-Diez, B.S. Parajón-Costa, N.A. Rey, Spectroscopic and theoretical study of the o-vanillin hydrazone of the mycobactericidal drug isoniazid, J. Mol. Struct. 1007 (2012) 95–101.
[64] S.R. Sheeja, N.A. Mangalam, M.P. Kurup, Y.S. Mary, K. Raju, H.T. Varghese, C.Y. Panicker, Vibrational spectroscopic studies and computational study of quinoline-2-carbaldehyde benzoyl hydrazone, J. Mol. Struct. 973 (2010) 36–46.

[65] N. Galić, A. Dijanošić, D. Kontrec, S. Miljanić, Structural investigation of aroylhydrazones in dimethylsulphoxide/water mixtures, Spectrochim. Acta. Part A. 95 (2012) 347–353.
[66] C. Arunagiri, A.G. Anitha, A. Subashini, S. Selvakumar, Synthesis, X-ray crystal structure, vibrational spectroscopy, DFT calculations, electronic properties and Hirshfeld analysis of (E)-4-Bromo-N'-(2, 4-dihydroxy-benzylidene) benzohydrazide, J. Mol. Struct. 1163 (2018) 368–378.
[67] T. Benković, A. Kenđel, J. Parlov-Vuković, D. Kontrec, V. Chiş, S. Miljanić, N. Galić, Aromatic hydrazones derived from nicotinic acid hydrazide as fluorimetric pH sensing molecules: structural analysis by computational and spectroscopic methods in solid phase and in solution, Spectrochim. Acta. Part A. 190 (2018) 259–267.
[68] M. Minteguiaga, E. Dellacassa, M.A. Iramain, C.A.N. Catalán, S.A. Brandán, FT-Raman FT-IR, UV–vis, NMR and structural studies of Carquejyl Acetate, a component of the essential oil from *Baccharis trimera* (Less.) DC. (Asteraceae), J. Mol. Struct. 1177 (2019) 499–510.
[69] J. Ruiz Hidalgo, A. Neske, M.A. Iramain, P.E. Alvarez, P. Leyton Bongiorno, S.A. Brandán, FT-IR, FT-Raman and UV-visible spectra of motrilin acetogenin isolated from *Annona cherimolia*, J. Mol. Struct. 1196 (2019) 508–517.
[70] F.L. Hirshfeld, Bonded-atom fragments for describing molecular charge densities, Theor. Chim. Acta 44 (1977) 129–138.
[71] M.A. Spackman, D. Jayatilaka, Hirshfeld surface analysis, CrystEngComm 11 (2009) 19–32.
[72] A.C. Anderson, The process of structure-based drug design, Chem. Biol. 10 (2003) 787–797.
[73] D. Gilbert, Bioinformatics software resources, Brief. Bioinform. 5 (2004) 300–304.
[74] A. Nagappan, J. Shin, M.H. Jung, Role of cannabinoid receptor type 1 in insulin resistance and its biological implications, Int. J. Mol. Sci. 20 (2019) 2109.
[75] E. Hernandez-Vazquez, S. Salgado-Barrera, J.J. Ramírez-Espinosa, S. Estrada-Soto, F. Hernández-Luis, Synthesis and molecular docking of N′-arylidene-5-(4-chlorophenyl)-1-(3, 4-dichlorophenyl)-4-methyl-1H-pyrazole-3-carbohydrazides as novel hypoglycemic and antioxidant dual agents, Bioorg. Med. Chem. 24 (2016) 2298–2306.
[76] https://www.rcsb.org/,in.